Published in final edited form as:

Nature. 2017 August 17; 548(7667): 343–346. doi:10.1038/nature23451.

Genome-scale Activation Screen Identifies a LncRNA Locus that Regulates a Gene Neighborhood

Julia Joung[1,2,3,4], **Jesse M. Engreitz**[2], **Silvana Konermann**[2,3,4], **Omar O. Abudayyeh**[2,3,4,5], **Vanessa K. Verdine**[2,3], **Francois Aguet**[2], **Jonathan S. Gootenberg**[2,3,4,6], **Neville E. Sanjana**[2,3,4], **Jason B. Wright**[2,3,4], **Charles P. Fulco**[2,6], **Yuen-Yi Tseng**[2], **Charles H. Yoon**[8], **Jesse S. Boehm**[2], **Eric S. Lander**[2,6,7,†], and **Feng Zhang**[1,2,3,4,†]

[1]Department of Biological Engineering, MIT, Cambridge, MA 02139, USA

[2]Broad Institute of MIT and Harvard, Cambridge, MA 02142, USA

[3]McGovern Institute for Brain Research at MIT, Cambridge, MA 02139, USA

[4]Department of Brain and Cognitive Science, MIT, Cambridge, MA 02139, USA

[5]Division of Health Sciences and Technology, MIT, Cambridge, MA 02139, USA

[6]Department of Systems Biology, Harvard Medical School, Boston, MA 02115, USA

[7]Department of Biology, MIT, Cambridge, MA 02139, USA

[8]Department of Surgery, Brigham and Women's Hospital, Boston, MA 02115, USA

Abstract

The mammalian genome contains thousands of loci that transcribe long noncoding RNAs (lncRNAs)[1-3], some of which are known to play critical roles in diverse cellular processes[4-7]. LncRNA loci can contribute to cellular regulation through a variety of mechanisms: while some encode RNAs that act non-locally (in *trans*)[6,8], emerging evidence indicates that many lncRNA loci act locally (in *cis*)—for example, through functions of the lncRNA promoter, the process of lncRNA transcription, or the lncRNA transcript itself in regulating the expression of nearby genes[7,9-11]. Despite their potentially important roles, it remains challenging to identify functional lncRNA loci and distinguish among these and other mechanisms. To address these challenges, we developed a genome-scale CRISPR-Cas9 activation screen targeting more than 10,000 lncRNA transcriptional start sites to identify noncoding loci that influence a phenotype of interest. We found 11 novel lncRNA loci that, upon recruitment of an activator, each mediate BRAF inhibitor resistance in melanoma. We investigated potential local and non-local mechanisms at these candidate loci and found that most appear to regulate nearby genes. Detailed analysis of one candidate, termed *EMICERI*, revealed that its transcriptional activation results in dosage-dependent activation of four neighboring protein-coding genes, one of which confers the resistance phenotype. Our screening and characterization approach provides a CRISPR toolkit to

[†]Correspondence should be addressed to zhang@broadinstitute.org (F.Z.) and lander@broadinstitute.org (E.S.L.).

Author contributions: J.J., S.K., and F.Z. conceived and designed the study. J.J., S.K., V.K.V., and J.S.G. performed experiments. J.J. analyzed data. O.O.A. and F.A. performed the analysis of clinical data sets. N.E.S. and J.B.W. performed ATAC-seq and ChIP experiments. J.M.E., C.P.F., and E.S.L. helped with lncRNA experimental design and interpretation. Y.Y.T., C.H.Y., and J.S.B. acquired and generated the Cancer Cell Line Factory models. J.J., J.M.E., E.S.L., and F.Z. wrote the paper with help from all authors.

systematically discover functions of noncoding loci and elucidate their diverse roles in gene regulation and cellular function.

We have previously used the Cas9 Synergistic Activation Mediator (SAM) to screen for protein-coding genes that confer resistance to the BRAF inhibitor vemurafenib in melanoma cells[12], making this an ideal phenotype for high-throughput screening of functional lncRNA loci (Supplementary Note 1). We designed a genome-scale sgRNA library targeting 10,504 unique intergenic lncRNA TSSs (>50 bp apart; see Methods, Supplementary Table 1)[2,13]. We transduced A375 (BRAF(V600E)) melanoma cells with the sgRNA library, cultured them in 2 μM vemurafenib or control (dimethyl sulfoxide, DMSO), and sequenced the distribution of sgRNAs after 14 days of drug treatment (Fig. 1a-b and Extended Data Fig. 1a). RIGER analysis[14] identified 16 significantly enriched candidate loci (FDR < 0.05, Fig. 1c,d, Extended Data Fig. 1b,c, and Supplementary Table 2), none of which had been previously functionally characterized.

To validate the screening results, we individually expressed the 3 most enriched sgRNAs targeting each of the top 16 candidate lncRNA loci in A375 cells. In all 16 cases, the sgRNAs conferred significant vemurafenib resistance (Extended Data Fig. 2), verifying the robustness of our screening approach. We performed RNA sequencing upon activation of each of the 11 loci with the strongest effects (Extended Data Fig. 2, Supplementary Table 3) and found global changes in gene expression consistent with vemurafenib resistance, supporting the functional relevance of these loci to the screening phenotype (Extended Data Fig. 3a).

Next, we turned to classifying the mechanisms by which activation of these loci might lead to resistance, which could include (i) a non-local function of the lncRNA transcript, (ii) a local function of the lncRNA transcript or its transcription; (iii) a local function of a DNA element in the lncRNA locus; and (iv) a local function of SAM, for example activating a nearby promoter (Supplementary Note 2). To focus on loci where the mechanism might require the lncRNA or its transcription (i and ii above), we activated each locus and detected a robust lncRNA transcript upregulation for 6 of these 11 loci (Fig. 1e, Supplementary Table 3). The remaining 5 loci may function through a mechanism other than activation of the lncRNA transcript (*e.g.*, iii and iv above; Supplementary Note 3 and Supplementary Table 4).

We explored whether activating each of these 6 lncRNA loci might affect vemurafenib resistance through non-local (i above) or local (ii and iii above) functions. To test whether candidate lncRNAs contribute to vemurafenib resistance via non-local functions, we overexpressed cDNAs encoding each lncRNA through random lentiviral integration and did not find any that affected drug resistance (Extended Data Fig. 3b), suggesting that these loci likely do not act through non-local functions (Supplementary Note 4 and Supplementary Table 3). To determine if the phenotype might result instead from local functions of the lncRNA loci in regulating a nearby gene[7,9,10], we examined the expression of all genes within 1 Mb of the targeted sites. At 5 of the 6 loci, we found that SAM targeting led to differential expression of between 1 and 8 nearby protein-coding genes (Supplementary Table 4; for remaining locus, see Supplementary Note 5). For example, activation of

NR_109890 upregulated its neighboring gene *EBF1* (Extended Data Fig. 3c), and activation of *TCONS_00015940* led to dosage-dependent upregulation of 4 neighboring protein-coding genes (Fig. 2a,b). Together, these analyses indicate that none of the lncRNA loci appear to confer vemurafenib resistance by producing *trans*-acting RNAs; rather, the loci may regulate the expression of one or more nearby genes.

To further dissect the mechanism for one of these candidate local regulators, we focused on *TCONS_00015940*, which, when targeted, led to a remarkable dosage-dependent activation of the 4 closest nearby genes (*EQTN*, *MOB3B, IFNK,* and *C9orf72*) (Fig. 2a,b). The targeted site is proximal to the boundary of a topological domain (Fig. 2a and Extended Data Fig. 4). Upon examining this locus, we found that *TCONS_00015940* is actually comprised of two separate transcripts (Extended Data Fig. 5a and Supplementary Note 6). We named these transcripts "*EQTN MOB3B IFNK C9orf72* enhancer RNA I", or *EMICERI,* and *EMICERII*. The *EMICERI* promoter, which we targeted in our screen, is actually the promoter for two genes, which are transcribed divergently and initiate ~66bp apart: *EMICERI* and *MOB3B*, a protein-coding gene (Fig. 2a). Tiling SAM across this region indicated that targeting a ~200 bp region activated both of these genes (Fig. 2a,c). In contrast, targeting SAM to the promoters of the other three nearby genes did not produce coordinated transcriptional activation in the region, although targeting the promoter of *C9orf72* led to a slight activation of *EMICERI* alone (Extended Data Fig. 5b and Supplementary Note 7). Together, these results demonstrate that the *EMICERI/MOB3B* promoter influences gene expression in a ~300 kb gene neighborhood.

To determine how coordinated upregulation of the *EMICERI* gene neighborhood led to vemurafenib resistance, we overexpressed the cDNA for each of the 4 protein-coding genes as well as *EMICERI or II* lncRNAs from randomly integrated lentivirus. Only *MOB3B* overexpression led to vemurafenib resistance (Fig. 3a and Extended Data Fig. 6a), indicating that although activation of the *EMICERI/MOB3B* promoter leads to transcriptional upregulation of 4 protein-coding genes and two lncRNA genes, overexpression of only one of these genes is sufficient for the resistance phenotype. Notably, *MOB3B,* a novel kinase activator of unknown function, is a paralog of *MOB1A/B*, known components of the Hippo signaling pathway, whose activation has been shown to confer vemurafenib resistance[15-18]. We found that *MOB3B* overexpression downregulates LATS1 to activate the Hippo signaling pathway (Fig. 3b,c, Extended Data Fig. 6f-h, and Supplementary Note 8). We extended our observations beyond the cell line used in our initial screen, by showing that activation of *EMICERI* and *MOB3B* conferred vemurafenib resistance in two additional sensitive melanoma cell lines (Fig. 3d,e, Extended Data Fig. 6i) and correlated with a gene-expression signature of vemurafenib resistance in melanoma patients from The Cancer Genome Atlas (Fig. 3f, Extended Data Fig. 3,7, and Supplementary Note 8). Together, these results indicate that activation of the *EMICERI* locus confers vemurafenib resistance via upregulation of *MOB3B* and subsequent activation of the Hippo signaling pathway.

As an aside, we sought to understand why *MOB3B* had not been identified in our previous SAM screen for protein-coding genes[12]. The explanation appears to be that the previous sgRNA library targeted *MOB3B* upstream of its TSS, whereas the optimal position for activation is downstream (Fig. 2c), and because resistance conferred by *MOB3B* activation

is weaker than for the top candidate genes in the previous screen (Extended Data Fig. 6b-e)[12].

We next considered whether transcriptional activation of *EMICERI* is required for full *MOB3B* upregulation. Alternatively, it is possible that targeting SAM to the shared *EMICERI/MOB3B* promoter may confer resistance only through direct activation of *MOB3B*. Accordingly, we used three perturbation methods to interfere with *EMICERI* transcription and observed effects on *MOB3B*:

i. To block transcription of *EMICERI*, we targeted dCas9 downstream of the *EMICERI* TSS. This intervention reduced the expression not only of *EMICERI*, but also of *MOB3B* and the other neighboring genes (Fig. 4a,b). We then used a bimodal perturbation system that uses an sgRNA without the SAM-recruitment sequences to target dCas9 to block *EMICERI* transcription and an sgRNA with the SAM-recruitment sequences to activate the promoter region (Fig. 4a, c). Different combinations of repression and activation sgRNAs targeting the *EMICERI* locus demonstrated that the transcriptional levels of *EMICERI* and *MOB3B* are tightly coupled across several orders of magnitude (correlation coefficient $r = 0.98$, $P < 0.0001$) (Fig. 4d).

ii. We generated clonal A375 cell lines carrying insertions of 3 tandem polyadenylation signals (pAS) downstream of the *EMICERI* TSS, which eliminated production of most of the *EMICERI* RNA without disrupting the promoter sequence (Fig. 4e, Extended Data Fig. 8a-c, and Supplementary Note 9). Upon SAM activation, the pAS-insertion clones showed significantly reduced expression of *EMICERI*, *MOB3B*, and the three other nearby genes compared to wild type clones (Fig. 4f, g and Extended Data Fig. 8d-f), and, as expected, reduced vemurafenib resistance (Fig. 4h and Extended Data Fig. 9). This provides genetic evidence that transcription of *EMICERI* is involved in *MOB3B* activation.

iii. We knocked down the *EMICERI* transcript by transient transfection with antisense oligonucleotides (ASOs), which can lead to RNase H-mediated cleavage of nascent transcripts and transcriptional termination of *EMICERI* (Fig. 4a and Supplementary Note 10)[19]. We performed these experiments in the context of activating *EMICERI* by targeting SAM to the promoter. ASOs targeting *EMICERI* reduced expression of both *EMICERI* and *MOB3B* in a dosage-dependent manner (Fig. 4i and Extended Data Fig. 10a), consistent with the dCas9 and pAS insertion results.

These *EMICERI* perturbation experiments demonstrate that transcription of *EMICERI* is required for full activation of *MOB3B*, confirming that *EMICERI* is a functional noncoding locus that activates four neighboring protein-coding genes and contributes to the screening phenotype.

Although the experiments above demonstrate that *EMICERI* transcription is required for *MOB3B* activation, the precise mechanism may involve either a function of the *EMICERI* transcript itself or the process of its transcription (*e.g.*, recruitment of transcriptional co-

activators)[10,20]. In the latter case, we might expect that *MOB3B* transcription would reciprocally regulate *EMICERI* expression. Indeed, we found that targeting dCas9 downstream of the *MOB3B* TSS successfully blocked *MOB3B* transcription and reduced expression of *EMICERI* and other neighboring genes (Extended Data Fig. 10b); and similarly, in the context of SAM activation, ASOs targeting *MOB3B* introns reduced the activation of both *MOB3B* and *EMICERI* (Fig. 4j and Extended Data Fig. 10c). Together, the *EMICERI* and *MOB3B* perturbation experiments suggested that transcription of both the lncRNA (*EMICERI*) and the mRNA (*MOB3B*) regulate one another in a positive feedback mechanism that then activates a broader gene neighborhood, potentially through general processes associated with transcription.

A major challenge in understanding the regulatory logic of the genome has been to identify functional lncRNA loci and characterize their mechanisms. Here we demonstrate that genome-scale activation screens enable systematic identification of many lncRNA loci that influence a specific cellular process, facilitating efforts to understand the functions and mechanisms of these key loci. Through a series of functional experiments, we provide a framework for distinguishing categories of regulatory mechanisms, including non-local (*trans*) functions as well as a diverse array of possible local regulatory mechanisms. Interestingly, the candidate lncRNA loci we identified appear to involve largely local, rather than non-local, regulation of gene expression (Supplementary Table 3), including a remarkable case involving coordinated activation of 4 nearby genes. Further application of this noncoding gain-of-function screening approach in other contexts, together with loss-of-function screening methods[21-24] and our characterization strategy, will help elucidate the complex roles of these poorly understood players in development and disease.

Methods

Design and cloning of SAM lncRNA library

RefSeq noncoding RNAs (Release 69) were filtered for lncRNA transcripts that were longer than 200 bp and not overlapping with RefSeq coding gene isoforms [13]. The RefSeq lncRNA catalog was combined with the Cabili lncRNA catalog and filtered for unique lncRNA transcriptional start sites (TSSs) defined as TSSs that were >50 bp apart [2]. This resulted in 10,504 unique lncRNA TSSs that were targeted with ~10 single guide RNAs (sgRNAs) each for a total library of 95,958 sgRNAs. sgRNAs were designed to target the first 800 bp upstream of each TSS and subsequently filtered for GC content >25%, minimal overlap of the target sequence, and homopolymer stretch <4 bp. After filtering, the remaining sgRNAs were scored according to predicted off-target matches as described previously [25], and 6 sgRNAs with the best off-target scores were selected in the first 200 bp region upstream of the TSS, 1 in the 200-300 bp region, 1 in the 300-400 bp region, 1 in the 400-600 bp region, and 1 in the 600-800 bp region. In regions with an insufficient number of possible sgRNAs, sgRNAs were selected from the neighboring region closer to the TSS. The ideal location for sgRNA targeting to achieve maximal activation, either upstream or downstream of the TSS, may be unique for each lncRNA locus and dependent on the local regulatory context (e.g., locations of TF binding sites). An additional 500 non-targeting sgRNAs from the GeCKO library [26] were included as controls. Cloning of the SAM sgRNA libraries was performed as

previously described with a minimum representation of 100 transformed colonies per sgRNA followed by next-generation sequencing (NGS) validation [27].

Lentivirus production and transduction

For transduction, plasmids were packaged into lentivirus via transfection of library plasmid with appropriate packaging plasmids (psPAX2: Addgene 12260; pMD2.G: Addgene 12259) using Lipofectamine 2000 (Thermo Fisher 11668019) and Plus reagent (Thermo Fisher 11514015) in HEK293FT (Thermo Fisher R70007) as described previously [27]. Human melanoma A375 cells (Sigma-Aldrich 88113005) were cultured in R10 media: RPMI 1640 (Thermo Fisher 61870) supplemented with 10% FBS (VWR 97068-085) and 1% penicillin/streptomycin (Thermo Fisher 15140122). Cells were passaged every other day at a 1:5 ratio. Concentrations for selection agents were determined using a kill curve: 300 μg/mL Zeocin (Thermo Fisher R25001), 10 μg/mL Blasticidin (Thermo Fisher A1113903), and 300 μg/mL Hygromycin (Thermo Fisher 10687010). Cells were transduced via spinfection and selected with the appropriate antibiotic as described previously [27]. During selection, media was refreshed when cells were passaged every 3 days. The duration of selection was 7 days for Zeocin and 5 days for Hygromycin and Blasticidin. Lentiviral titers were calculated by spinfecting cells with 5 different volumes of lentivirus and determining viability after a complete selection of 3 days [27].

Vemurafenib resistance screen

The vemurafenib resistance screen was conducted similarly to a previously described genome-scale SAM coding gene screen [12]. A375 stably integrated with dCas9-VP64 (Addgene 61425) and MS2-P65-HSF1 (Addgene 61426) were transduced with the pooled sgRNA library (Addgene 61427) as described above at an MOI of 0.3 for a total of 4 infection replicates, with a minimal representation of 500 transduced cells per sgRNA in each replicate. Cells were maintained at >500 cells per sgRNA during subsequent passaging. After 7 days of Zeocin selection and 2 days of no antibiotic selection, cells were split into control (DMSO) and vemurafenib (2 μM PLX-4720 dissolved in DMSO, Selleckchem S1152) conditions. Cells were passaged every 2 days for a total of 14 days of control or vemurafenib treatment. The 14-day screening duration was selected based on previous studies [12,23,26]. At the end of the screening selection, >500 cells per sgRNA in each condition were harvested for gDNA extraction and amplification of the virally integrated sgRNAs as described previously [27]. Resulting libraries were deep-sequenced on Illumina MiSeq or NextSeq platforms with a coverage of >25 million reads passing filter per library.

NGS and screen hits analysis

NGS data was de-multiplexed using unique index reads. sgRNA counts were determined based on perfectly matched sequencing reads only. For each condition, a pseudocount of 1 was added to the sgRNA count and the counts were normalized to the total number of counts in the condition. The sgRNA fold change as a result of screening selection was calculated by dividing the normalized sgRNA counts in the vemurafenib condition by the control and taking the base 2 logarithm. RIGER [14] analysis was performed using GENE-E based on the normalized $\log_2$ ratios for each infection replicate. Since a low percentage of functional sgRNAs was expected for each lncRNA loci, the weighted sum method was used. To

determine the empirical false discovery rate (FDR) of candidate lncRNA loci, the weighted sum for 10 randomly selected non-targeting sgRNAs in the sgRNA library was used to estimate the *P* value for each lncRNA locus and a threshold based on a FDR of 0.05 (Benjamini-Hochberg) was selected that corresponded to a *P* value of 0.031. 7 candidate lncRNA loci were selected based on the average ranking between infection replicates 1 and 2, and 9 candidate lncRNA loci were selected based on the average ranking in all 4 infection replicates. All candidate lncRNA loci had *P* value < 10^{-5}.

Vemurafenib resistance assay

A375 cells stably integrated with dCas9-VP64 and MS2-P65-HSF1 were transduced with individual sgRNAs targeting the 16 top candidate lncRNA loci from the vemurafenib resistance screen (3 sgRNAs with the highest enrichment per lncRNA locus; Supplementary Table 5) or with control non-targeting sgRNA at an MOI of <0.5 and selected with Zeocin for 5 days as described above. For cDNA overexpression, A375 cells were transduced with cDNA (Supplementary Table 7) or control GFP at an MOI of <0.5 and selected with Hygromycin for 4 days. At 5 days post transduction, cells were replated at low density (3×10^3 cells per well in a 96-well plate). 2 μM vemurafenib or control DMSO was added 3h after plating and refreshed every 2 days for 3-4 days before cell viability was measured using CellTiter-Glo Luminescent Cell Viability Assay (Promega G7571). Significance testing was performed using Student's *t*-test. For primary patient tumor-derived melanoma cell lines, cells were plated at low density (2×10^3 cells per well in a 96-well plate) and vemurafenib was added 24h after plating. Cells were treated for 3 days before cell viability was measured. For vemurafenib dose response curves, the indicated concentrations of vemurafenib were added and the normalized percent survival values were fitted with a nonlinear curve (log(inhibitor) vs normalized response; Prism 6). Significant differences in logIC50 values was determined using the extra sum-of-squares F test.

qPCR quantification of transcript expression

A375 cells stably integrated with SAM components were transduced with individual sgRNAs targeting top candidate lncRNA loci (Supplementary Table 5), perturbing the *EMICERI* locus (Supplementary Table 8), or non-targeting control at an MOI of <0.5 and selected with Zeocin for 5 days as described above. For cDNA overexpression, A375 cells were transduced with cDNA (Supplementary Table 7) or control GFP at an MOI of <0.5 and selected with Hygromycin for 4 days. Cells were plated at 5 days post transduction at 70% confluency (3×10^4 cells per well in a 96-well plate), and harvested for RNA 24h after plating as described previously [27]. For transcripts that this method could not detect, cells transduced with the respective sgRNAs were plated at 5 days post transduction (1.8×10^5 cells per well in a 24-well plate). RNA was harvested using the RNeasy Plus Mini Kit (Qiagen 74134) and 1 μg of RNA was used for reverse transcription with the qScript Flex cDNA Kit (VWR 95049) and lncRNA-specific primers (Supplementary Table 6). After reverse transcription, TaqMan qPCR was performed with custom or readymade probes as described previously (Supplementary Table 7) [27]. Significance testing was performed using Student's *t*-test.

RNA sequencing and data analysis

A375 cells transduced with individual sgRNAs targeting candidate lncRNA loci or with control non-targeting sgRNAs (Supplementary Table 5) were plated 5 days post transduction at 9×10^4 cells per well or 1.8×10^5 cells per well respectively in a 24-well plate. 3 bioreps per condition were plated. For cDNA overexpression, A375 cells were transduced with cDNA (Supplementary Table 7) or control GFP at an MOI of <0.5 and selected with Hygromycin for 4 days. Cells were treated with 2 μM vemurafenib for 3 days before RNA was harvested as described above. The 6 candidate lncRNA loci with detectable transcript upregulation were prepped with TruSeq Stranded Total RNA Sample Prep Kit with Ribo-Zero Gold (Illumina RS-122-2302) and all other samples were prepped with NEBNext Ultra RNA Library Prep Kit for Illumina (NEB E7530S) and NEBNext PAS mRNA Magnetic Isolation Module (NEB E7490S). Libraries were deep-sequenced on the Illumina NextSeq platform (>9 million reads per condition). Bowtie [28] index was created based on the human hg19 UCSC genome and known gene and lncRNA transcriptome constructed as described above. Paired-end reads were aligned directly to this index using Bowtie with command line options "-q --phred33-quals -n 2 -e 99999999 -l 25 -I 1 -X 1000 --chunkmbs 512 -p 1 -a -m 200 -S". Next, RSEM v1.2.22 [29] was run with default parameters on the alignments created by Bowtie to estimate expression levels.

RSEM's TPM estimates for each transcript were transformed to log-space by taking $\log_2$(TPM+1). Transcripts were considered detected if their transformed expression level was equal to or above 1 (in $\log_2$(TPM+1) scale). All genes detected in at least one library (out of three libraries per condition) were used to find differentially expressed genes. For lncRNA loci activation, the Student's *t*-test was performed on each of the 3 replicates for each targeting sgRNA against both non-targeting sgRNAs. For *MOB3B* cDNA overexpression, the *t*-test was performed on the cDNA overexpression against GFP control. Only genes that were significant (*p*-value pass 0.05 FDR correction) were reported. For lncRNA loci activation, the genes overlapping all 3 targeting sgRNAs were reported as differentially expressed as a result of lncRNA loci activation. Power analysis for two-sided *t*-test were performed on each targeting sgRNA against both non-targeting sgRNAs to determine the probability of correctly identifying a gene as differentially expressed.

For annotating *EMICERI*, TopHat [30] was used to align RNA-seq reads from A375 transduced with sgRNA 2 or sgRNA 3 (Supplementary Table 8) with command line options "--solexa-quals --num-threads 8 --library-type fr-firststrand --transcriptome-max-hits 1 --prefilter-multihits --keep-fasta-order". To further investigate the mechanism for *MOB3B* overexpression, Ingenuity Pathway Analysis was applied to all genes differentially expressed with at least 1.2-fold change or less than 0.7-fold change and the most likely upstream regulator was reported.

Hi-C and chromatin immunoprecipitation with sequencing (ChIP-seq) in GM12878

In situ Hi-C data for GM12878 was obtained and visualized using 2.5kb-resolution KL-normalized observed matrix [31]. Hi-C data from 7 cell lines suggested similar topological domain annotations as GM12878 (Rao et al. *Cell* 2014), suggesting that the TAD present in GM12878 is consistent across cell types. CTCF ChIP-seq for GM12878 and hg19 generated

by the ENCODE Project Consortium [32] was downloaded from UCSC Genome Browser. CTCF motifs were identified using FIMO [33] to search for the “V_CTCF_01” and “V_CTCF_02” position weight matrices from TRANSFAC [34] as described previously [21].

Assay for transposable and accessible chromatin sequencing (ATAC-seq)

ATAC-seq samples were prepared as described previously [23]. A375 cells were cultured in R10 as described above and 5×10^4 cells in log-phase growth were harvested using an existing ATAC library preparation protocol with minor modifications [35]. Library was sequenced using the Illumina NextSeq platform at ~136 million paired-end reads. Samples were aligned to the human hg19 UCSC genome using Bowtie [28] with command line options “--chunkmbs 256 -p 24 -S -m 1 -X 2000”. For quality control, the duplicate read rate was measured using Picard-Tools Mark Duplicates (10-30%) and the mitochondrial read rate was measured by Bowtie alignment to chrM (<5%) [36].

PhastCons sequence conservation

PhastCons data for primates (n=10 animals), placental mammals (n=33), and vertebrates (n=46) for hg19 were downloaded from UCSC Genome Browser and aligned to the *EMICERI* locus [37].

ChIP-seq for histone modifications

ChIP samples were prepared as described previously [23]. Briefly, A375 cells were plated in T-225 flasks and grown to 70-90% confluence. Formaldehyde was added directly to the growth media for a final concentration of 1% for 10 mins at 37°C to initiate chromatin fixation. The entire two-day ChIP procedure was performed using the EZ-Magna ChIP HiSens Chromatin Immunoprecipitation Kit (Millipore 1710460) according to the manufacturer's protocol. Samples were pulse sonicated with 2 rounds of 10 mins (30s on-off cycles, high frequency) in a rotating water bath sonicator (Diagenode Bioruptor) with 5 mins on ice between each round. To detect histone modifications, antibodies (H3K4me2: Millipore 17-677, H3K4me3: Millipore 04-745, H3K27ac: Millipore 17-683) were optimized individually for each antibody to be 0.5 μL for 1 million cells. 1 μL of IgG (Millipore 12-370) was used for negative control.

After verifying that the IgG ChIP had minimal background, ChIP samples were prepped with NEBNext Ultra II DNA Library Prep Kit for Illumina (NEB E7645S) and deep-sequenced on the Illumina NextSeq platform (>60 million reads per condition). Bowtie [28] was used to align paired-end reads to the human hg19 UCSC genome with command line options “-q -X 500 --sam --chunkmbs 512”. Next, Model-based analysis of ChIP-seq (MACS) [38] was run with command line options “-g hs -B -S --call-subpeaks” to identify histone modifications.

Western blot

A375 cells transduced with *MOB3B* cDNA or GFP control were plated 5 days post transduction at 1.8×10^5 cells per well in a 24-well plate. Cells were treated with 2 μM vemurafenib for 6, 12, 24, or 48 h before protein lysates were harvested with RIPA lysis buffer (Cell Signaling Technologies 9806S) containing protease inhibitor (Roche

05892791001) and phosphatase inhibitor (Cell Signaling Technologies 5870S) cocktails. Samples standardized for protein concentration with the Pierce BCA protein assay (Thermo Fisher 23227) were incubated at 70°C for 10 mins under reducing conditions. After denaturation, 10 μg of the samples were separated by Bolt 4-12% Bis-Tris Plus Gels (Thermo Fisher NW04120BOX) and transferred onto a polyvinylidene difluoride membrane using iBlot Transfer Stacks (Thermo Fisher IB401001). Blots were blocked with Odyssey Blocking Buffer (TBS; LiCOr 927-50000) and probed with different primary antibodies [anti-pERK (Cell Signaling Technologies 4370, 1:2000 dilution), anti-ERK (Cell Signaling Technologies 4695, 1:1000 dilution), anti-pAKT (Ser473, Cell Signaling Technologies 4060, 1:1000 dilution), anti-AKT (Cell Signaling Technologies 4691, 1:1000 dilution), anti-LATS1 (Cell Signaling Technologies 3477, 1:1000 dilution), anti-YAP/TAZ (Cell Signaling Technologies 8418, 1:1000 dilution), anti-MST1 (Cell Signaling Technologies 3682, 1:1000 dilution), anti-ACTB (Sigma A5441, 1:5000 dilution)] overnight at 4°C. Blots were then incubated with secondary antibodies IRDye 680RD Donkey anti-Mouse IgG (LiCOr 925-68072) and IRDye 800CW Donkey anti-Rabbit IgG (LiCOr 925-32213) at 1:20,000 dilution in Odyssey Blocking Buffer for 1 hr at room temperature. p-ERK and p-AKT blots were stripped with Restore PLUS Western Blot Stripping Buffer (Thermo Fisher 46430) before probing for ERK and AKT respectively. Blots were imaged using the Odyssey CLx (LiCOr).

Primary patient melanoma-derived cell lines

CLF_SKCM_001_T and CLF_SKCM_004_T melanoma tumor tissues were obtained from Dana-Farber Cancer Institute hospital with informed consent and the cancer cell model line generation was approved by the ethical committee. Tumor tissues were dissected into tiny pieces by scalpers around 100 times. Dissected tissues were dissociated in the collagenase/hyaluronidase (STEMCELL technologies 07912) medium for 1 hour. The red blood cells were further depleted by adding the Ammonium Chloride Solution (STEMCELL technologies 07800). The dissociated cells were plated with the smooth muscle growing medium-2 (Lonza CC-3181) in the six well plate and split when the well confluency reached to 80%. Cells were passaged for 5 times with 1:4 splitting ratio for a sequencing verification. The confirmed BRAF V600E melanoma cell models were be propagated for another 7-15 passages and cryovial preserved. We used passage 12 cells for this study. All cells were refed every 3-4 days.

Gene expression and pharmacological validation analysis

Gene expression data (CCLE, TCGA) and pharmacological data (CCLE) were analyzed to better understand the biological relevance of *EMICERI* and *MOB3B*. Transcript expression in TCGA and CCLE samples was quantified as follows: 1) FASTQ files were generated from available BAM files using SamToFastq in Picard Tools (https://broadinstitute.github.io/picard/); 2) reads were aligned with STAR v2.5.2b [39] using parameters from the GTEx Consortium pipeline (https://github.com/broadinstitute/gtex-pipeline) and genome indexes generated for read lengths of 48bp (TCGA) and 101bp (CCLE) (--sjdbOverhang option); 3) expression was quantified using RSEM v1.2.22 [29]. For the alignment and quantification steps, annotations for *TCONS_00011252*, *NR_034078*, *TCONS_00010506*, *TCONS_00026344*, *TCONS_00015940_1*, *TCONS_00015940_2*, and *NR_109890* were

appended to the GENCODE 19 GTF (https://www.gencodegenes.org/releases/19.html). Gene-level quantifications were also calculated with RNA-SeQC [40] to validate the RSEM results.

Gene expression (RNA-sequencing) were collected from 113 $BRAF^{V600}$-mutant primary and metastatic patient tumors from The Cancer Genome Atlas (TCGA: https://tcga-data.nci.nih.gov/tcga/). Because pharmacological data was not available for the TCGA melanoma samples, signature gene sets, including some from the Molecular Signature Database (MSigDB) [41], were used to fully map the transcriptional BRAF-inhibitor resistant/sensitive states in TCGA as previously described [42]. The TCGA dataset was used for determining the association between resistance and the expression of candidate lncRNA loci or genes in the *EMICERI* locus. Additionally, we sought a more robust scoring system independent of any single gene. Gene expression signatures were generated based on the genes that were differentially expressed (top 1000 most differentially expressed) as a result of candidate lncRNA loci or *MOB3B* overexpression identified from RNA-seq. Using single-sample Gene Set Enrichment Analysis (ssGSEA) [43], a score was generated for each sample that represents the enrichment of the gene expression signature in that sample and the extent to which those genes are coordinately up- or down-regulated. Patient tumors were also sorted by *EMICERI* expression to determine correlation between expression of *EMICERI* and its neighboring genes.

In the CCLE dataset [44], gene expression data (RNA-sequencing, GCHub: https://cghub.ucsc.edu/datasets/ccle.html) and pharmacological data (activity area for MAPK pathway inhibitors) from $BRAF^{V600}$ mutant melanoma cell lines were used to compute the association between PLX-4720 resistance and the expression of genes in the *EMICERI* locus. Similar to the TCGA analysis, the *MOB3B* overexpression gene signature was determined using ssGSEA [43] projected onto the CCLE RNA-sequencing dataset. Cell lines were also sorted by *EMICERI* expression to determine correlation between expression of *EMICERI* and its neighboring genes.

To measure correlations between different features (signature scores, gene expression, or drug-resistance data) in the external cancer datasets, an information-theoretic approach (Information Coefficient; IC) was used and significance was measured using a permutation test (n=10,000), as previously described [42]. The IC was calculated between the feature used to sort the samples (columns) in each dataset and each of the features plotted in the heat map (pharmacological data, gene expression, and signature scores).

Polyadenylation signal (pAS) insertion

To truncate *EMICERI*, the following pAS sequences were inserted consecutively 103, 156, and 198 bp downstream of each copy of *EMICERI*'s TSS:

Synthetic pAS—

AATAAAAGATCTTTATTTTCATTAGATCTGTGTGTTGGTTTTTTGTGTG

SV40 pAS—

GTTTATTGCAGCTTATAATGGTTACAAATAAAGCAATAGCATCACAAATTTCACAAA

TAAAGCATTTTTTTCACTGCATTCTAGTTGTGGTTTGTCCAAACTCATCAATGTATC
TTATCATGTCT

PGK pAS—

AAATTGATGATCTATTAAACAATAAAGATGTCCACTAAAATGGAAGTTTTTTCCTG
TCATACTTTGTTAAGAAGGGTGAGAACAGAGTACCTACATTTTGAATGGAAGGATT
GGAGCTACGGGGGTGGGGGTGGGGTGGGATTAGATAAATGCCTGCTCTTTACTGA
AGGCTCTTTACTATTGCTTTATGATAATGTTTCATAGTTGGATATCATAATTTAAACA
AGCAAAACCAAATTAAGGGCCAGCTCATTCCTCCACTCACGATCTATA

PAS clones were generated using CRISPR-Cas9 mediated homology-directed repair (HDR). 3 different sgRNAs targeting 103, 156, and 198 bp downstream of *EMICERI* (HDR sgRNA 1-3, Supplementary Table 9) and corresponding pAS HDR plasmids were used for inserting pAS into each of the 3 copies of *EMICERI* in A375. To construct the PAS HDR plasmids, for each sgRNA the HDR templates that consisted of the 850-900 bp genomic regions flanking the sgRNA cleave site were PCR amplified from A375 genomic DNA using KAPA HiFi HotStart Readymix (KAPA Biosystems KK2602). Then 3 pAS sequences (in the order listed above) flanked by the HDR templates were cloned into pUC19 (Addgene 50005). To insert pAS downstream of *EMICERI*s TSS, 3 rounds of HDR were performed with a different sgRNA and respective pAS HDR plasmid at each round such that selected clones contained pAS sequences in 1 copy of *EMICERI* in the first round, 2 copies in the second round, and 3 copies in the third round. At each round of HDR, A375 cells were nucleofected with 4 μg of sgRNA and Cas9 plasmid (Addgene 52961) and 2.5 μg of pAS HDR plasmid using SF Cell Line 4D-Nucleofector X Kit L (Lonza V4XC-2024) according to the manufacturer's instructions. Cells were then seeded sparsely (5×10^4 cells per 10-cm Petri dish) to form single-cell clones. After 24h, cells were selected for Cas9 expression with 1 μg/mL Puromycin for 2 days and expanded until colonies can be picked (~5 days).

To pick colonies, cells were detached by replacing the media with PBS and incubating at room temperature for 15 mins. Each cell colony was removed from the Petri dish using a 200 μL pipette tip and transferred a well in a 96-well plate for expansion. Clones with pAS insertions were identified by 2-round PCR amplification (Supplementary Table 9), first with primers amplifying outside of the HDR template (HDR primer F1 and HDR primer R, 15 cycles) and then with primers amplifying the region of insertion (HDR primer F2 and HDR primer R, 15 cycles) to avoid detecting the HDR template plasmid as a false positive. Products were run on a gel to identify insertions and Sanger sequencing confirmed that the pAS sequences had been inserted at the appropriate site. During each round of HDR, 3 clones with pAS insertions and 1 clone without pAS insertion (wild type) were selected for further expansion and characterization. The wild type clone controls for potential on- and off-target indels.

Antisense oligonucleotide (ASO) knockdown

ASOs targeting *EMICERI/II* and *MOB3B* were custom designed using Exiqon's Antisense LNA GapmeR designer (Supplementary Table 10) and a non-targeting ASO (Exiqon 300610) was included for control. ASOs were resuspended in water to a final concentration of 100 μM. A375 stably expressing SAM components dCas9-VP64 and MS2-p65-HSF1

were nucleofected with 500 ng sgRNA (Supplementary Table 8; Addgene 73795) and 100 pmol ASO using the SF Cell Line 4D-Nucleofector X Kit S (Lonza V4XC-2032) according to the manufacturer's instructions. Cells were then seeded at 3×10^4 cells per well in a 96-well plate. 24h after nucleofection, cells were selected for the sgRNA plasmid with 1 μg/mL Puromycin (Thermo Fisher A1113803) for 2 days and changes in transcript expression were determined by qPCR as described above.

Code availability

Code for the analyses described in this paper is available from the authors upon request.

Extended Data

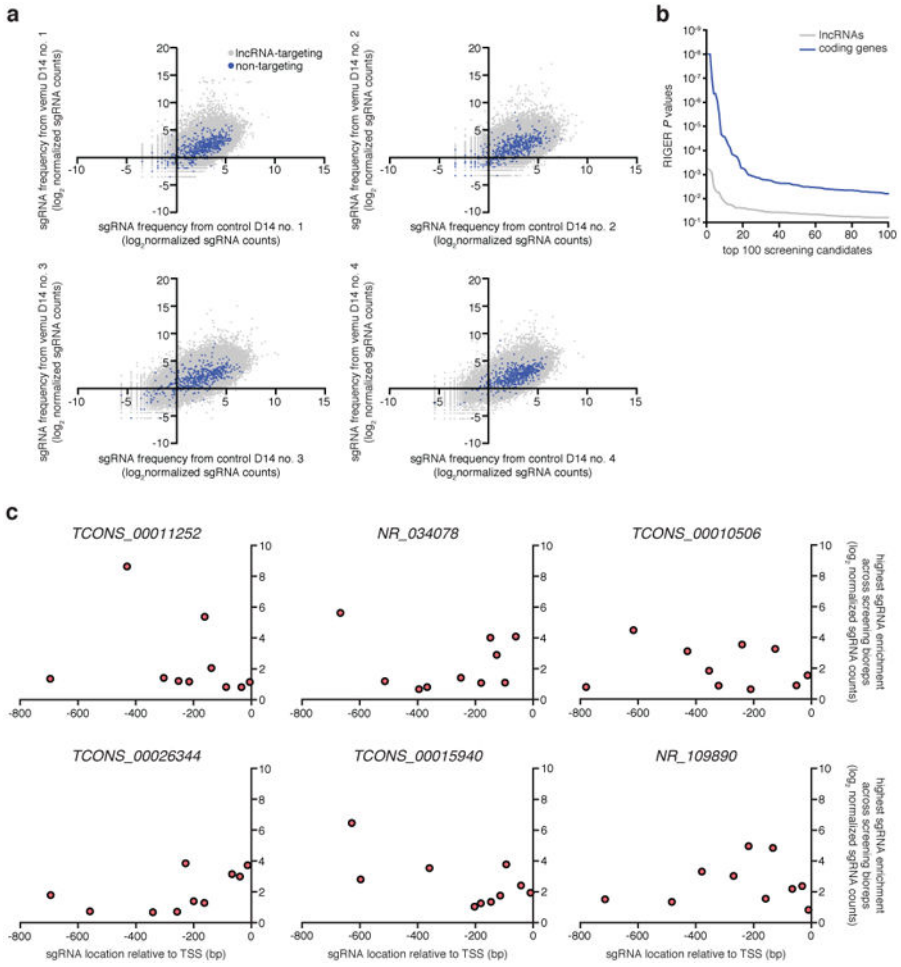

Extended Data Figure 1. Genome-scale activation screen for lncRNA loci involved in BRAF inhibitor resistance

a, Scatterplots showing lncRNA-targeting and non-targeting sgRNA frequencies after vemurafenib (vemu) or control treatment from n = 4 infection replicates. **b,** RIGER *P* values for the top 100 hits from the previous SAM protein-coding gene screen [12] compared to the SAM lncRNA loci screen. **c,** For each candidate lncRNA locus, 10 sgRNAs were designed to target the proximal promoter region (800 bp upstream of the TSS). The relationship

between the highest sgRNA enrichment in vemurafenib-treated compared to control condition across screening bioreps (n = 4) and respective spacer position suggests that sgRNAs targeting closer to the annotated TSS are not necessarily more effective, consistent with previous results [12].

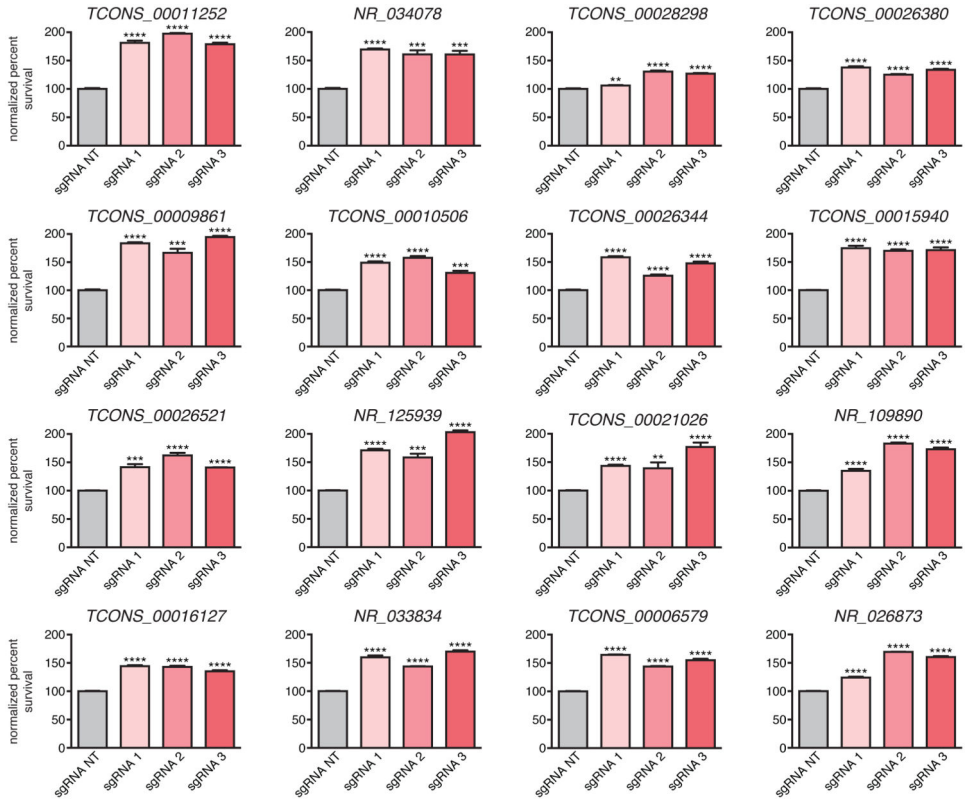

Extended Data Figure 2. Validation of candidate lncRNA loci for vemurafenib resistance

Vemurafenib resistance for A375 transduced with SAM and individual sgRNAs targeting the top 16 candidate lncRNA loci normalized to a non-targeting (NT) sgRNA. All values are mean ± SEM with n = 4. **** $P < 0.0001$; *** $P < 0.001$; ** $P < 0.01$.

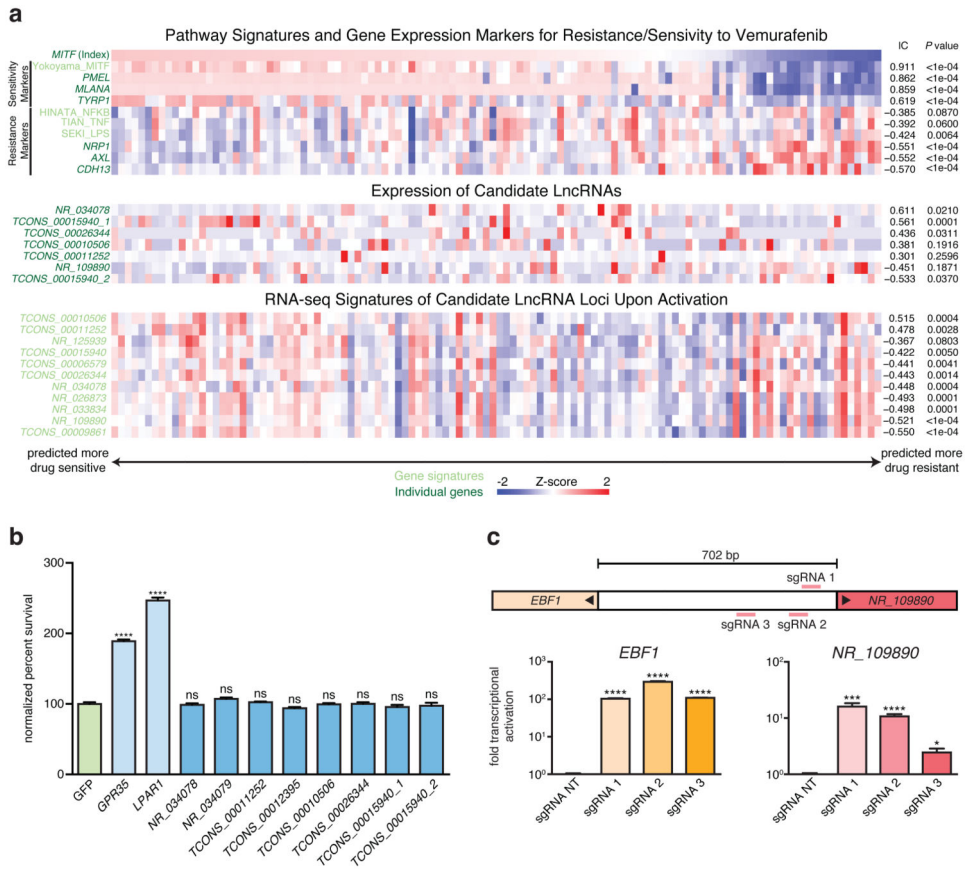

Extended Data Figure 3. Activation of candidate lncRNA loci mediate vemurafenib resistance by potentially acting locally to regulate expression of nearby genes

a, Heat map showing expression of gene/signature markers for BRAF inhibitor sensitivity (top), expression of candidate lncRNA loci (middle), and RNA-seq signature of gene expression changes upon activation of candidate lncRNA loci (bottom) in 113 different BRAF (V600) patient melanoma samples (primary or metastatic) from The Cancer Genome Atlas. All associations are measured using the information coefficient (IC) between the index and each of the features and *P* values are determined using a permutation test. Panels show Z scores. **b,** Vemurafenib resistance of A375 cells overexpressing each candidate lncRNA cDNA or protein-coding gene normalized to GFP. *GPR35* and *LPAR1* are positive controls identified previously [12]. The same set of sgRNAs targeted *TCONS_00012395* and *TCONS_00011252*; *NR_034078* and *NR_034079*; *TCONS_00015940_1* and *TCONS_00015940_2*. **c,** Expression of *NR_109890* and its neighboring gene *EBF1* after SAM activation of *NR_109890*. All values are mean ± SEM with n = 4. *****P* < 0.0001; ****P* < 0.001; **P* < 0.05. ns = not significant.

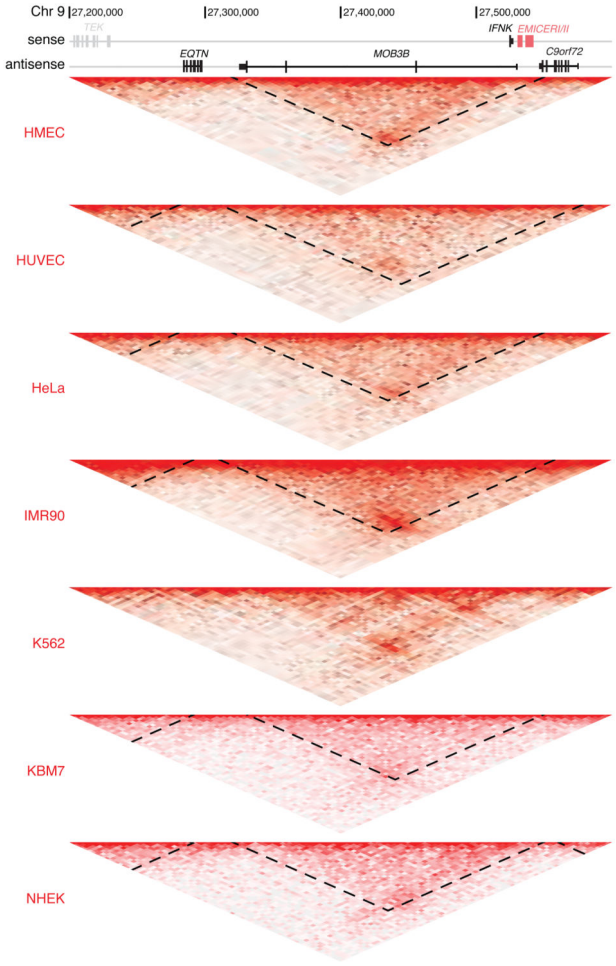

Extended Data Figure 4. Topological domain in the *EMICERI* locus is consistent across cell types

Hi-C data and topological domain annotations (dotted lines) in the *EMICERI* locus from 7 cell lines [31]. Heat map shows KR-normalized contact matrix at 5-kb resolution. Domain annotations for chromosome 9 were not available in K562, but the same topological domain structure is evident.

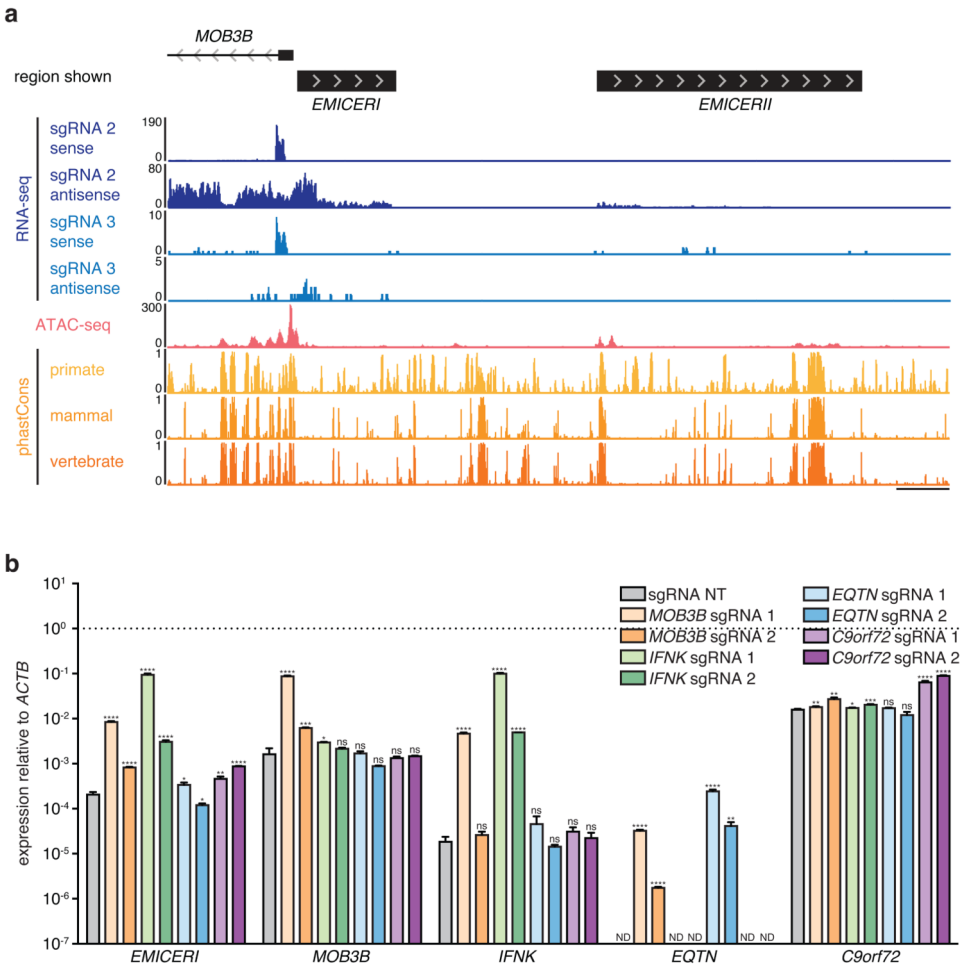

Extended Data Figure 5. Dosage-dependent upregulation of the *EMICERI* locus is specific to activation of *EMICERI* at its conserved regulatory element

a, TopHat alignment of RNA-seq paired-end reads suggests that *EMICERI* is located at chr9:27,529,917-27,531,782 and *EMICERII* at chr9:27,535,711-27,540,711 (UCSC hg19) (Supplementary Note 6). A375 ATAC-seq and phastCons conservation scores for primates, placental mammals, and vertebrates at the *EMICERI* locus. Scale bar, 1 kb. **b,** Expression of *EMICERI* and its neighboring genes *MOB3B*, *IFNK*, *EQTN*, and *C9orf72* after transduction with sgRNAs targeting SAM to the promoters of neighboring genes. All values are mean ± SEM with n = 4. ****$P < 0.0001$; ***$P < 0.001$; **$P < 0.01$; *$P < 0.05$. ns = not significant. ND = not detected.

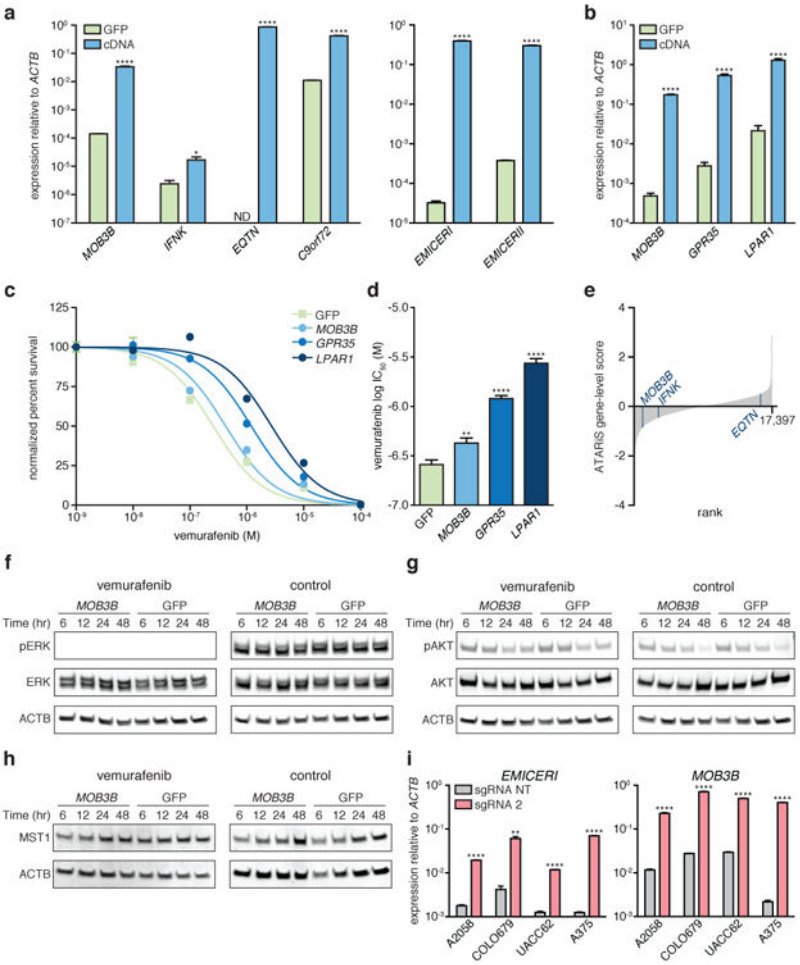

Extended Data Figure 6. Activation of *EMICERI* mediates vemurafenib resistance through *MOB3B*

a, Expression of the neighboring genes or *EMICERI/II* after cDNA overexpression compared to GFP control. **b,** cDNA overexpression of top hits from the SAM protein-coding gene screen for vemurafenib resistance (*GPR35* and *LPAR1*) [12] or *MOB3B* compared to GFP control. **c,** Vemurafenib dose response curves for A375 cells overexpressing cDNA or GFP control. **d,** Vemurafenib half maximal inhibitory concentration (IC50) for the same conditions in (c). **e,** ATARiS gene-level scores from the Achilles Project that reflect genetic vulnerabilities of A375. Lower ATARiS gene-level scores indicate stronger dependency on the gene. Rank of *MOB3B*, 1,084; *IFNK*, 3,078; *EQTN*, 15,939. **f** to **h,** Western blots of A375 stably overexpressing *MOB3B* cDNA or GFP control after vemurafenib or control (DMSO) treatment. **i,** Expression of *EMICERI* and *MOB3B* after SAM activation in different melanoma cell lines. All values are mean ± SEM with n = 4. *****P* < 0.0001; ***P* < 0.01; **P* < 0.05. ND = not detected.

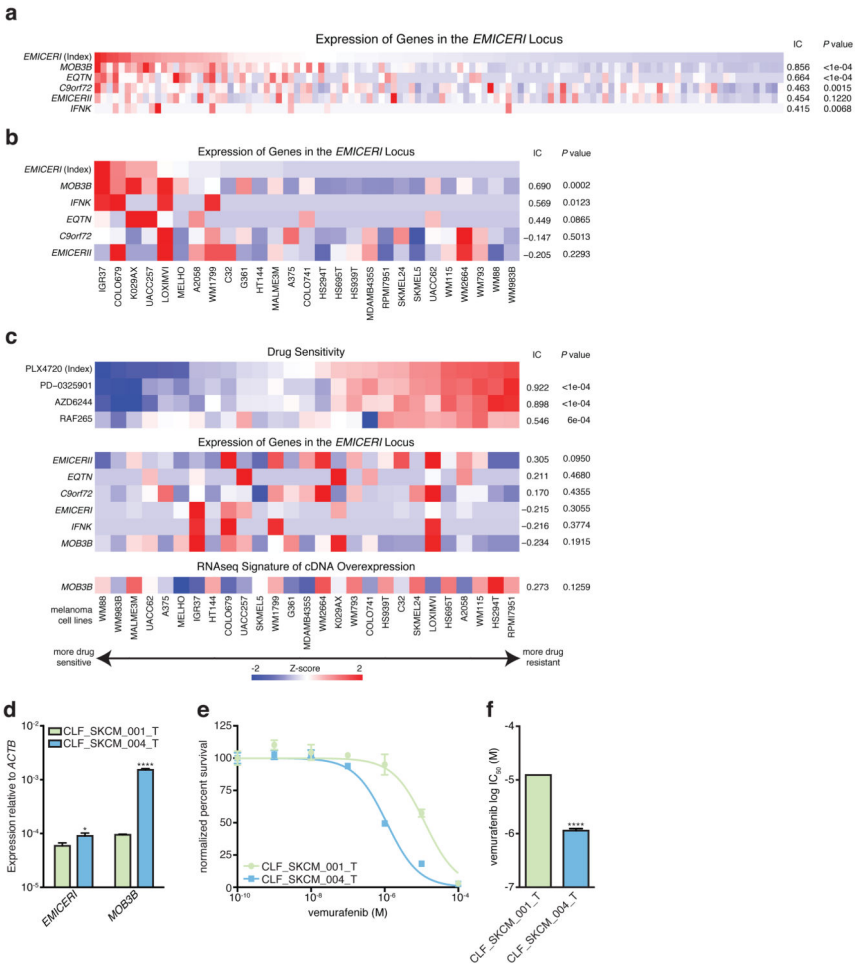

Extended Data Figure 7. *EMICERI* expression is strongly correlated with *MOB3B* expression and vemurafenib sensitivity in melanoma cell lines and patient samples

a, Heat map showing expression of genes in the *EMICERI* locus in 113 different BRAF (V600) patient melanoma samples (primary or metastatic) from The Cancer Genome Atlas. Samples are sorted by *EMICERI* expression. **b,** Heat map showing expression of genes in the *EMICERI* locus in melanoma cell lines from the Cancer Cell Line Encyclopedia (CCLE) sorted by *EMICERI* expression. **c,** Heat map showing sensitivity to different drugs (top), expression of genes in the *EMICERI* locus (middle), and *MOB3B* cDNA overexpression RNA-seq signature (bottom; see Methods for signature generation) in melanoma cell lines from CCLE. Drug sensitivities are measured as Activity Areas. The melanoma cell lines are sorted by PLX-4720 (vemurafenib) drug sensitivity. RAF inhibitors: PLX-4720 and RAF265; MEK inhibitors: AZD6244 and PD-0325901. **d,** Expression of *EMICERI* and *MOB3B* in two primary patient-derived BRAF(V600E) melanoma cell lines. **e,** Vemurafenib dose response curves for the same cell lines. **f,** Vemurafenib half maximal inhibitory concentration (IC50) for the same conditions as (e). All associations are measured using the information coefficient (IC) between the index and each of the features and *P* values are determined using a permutation test. Heat maps show Z scores. All values are mean ± SEM with n = 4. ****$P < 0.0001$; *$P < 0.05$.

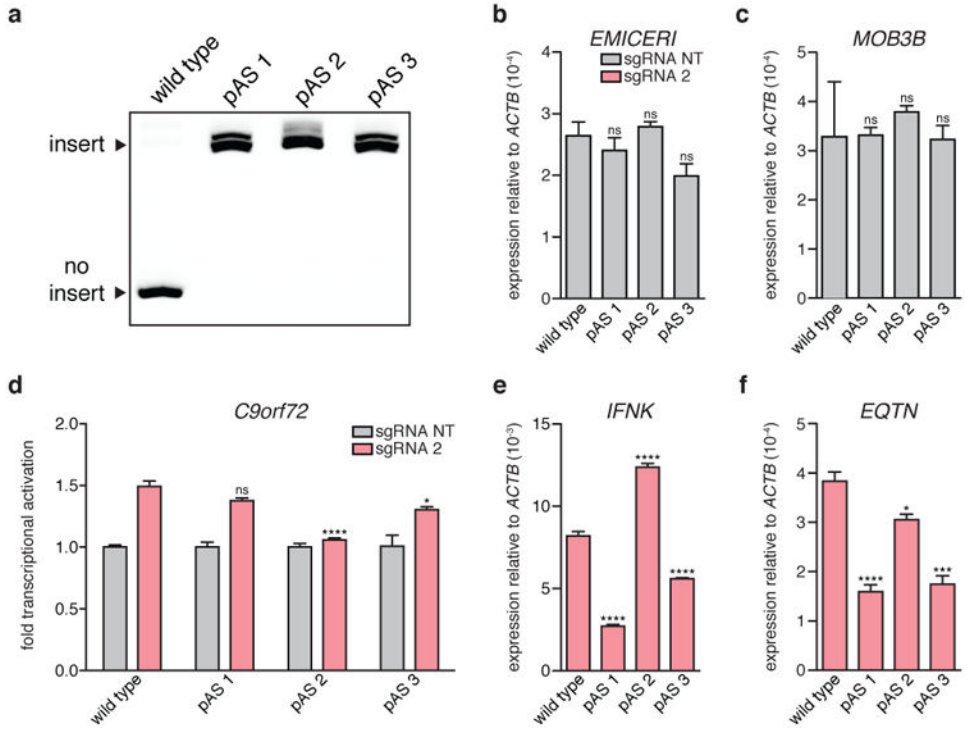

Extended Data Figure 8. Transcriptional activation of *EMICERI* modulates expression of neighboring genes

a, Gel confirming polyadenylation signal (pAS) insertion into all 3 copies of *EMICERI* for each pAS clone. **b** to **c,** Basal expression of *EMICERI* and *MOB3B* for the wild type and pAS clones. **d** to **f,** Expression of *C9orf72*, *IFNK*, and *EQTN* after targeting SAM to *EMICERI* for the wild type and pAS clones. All values are mean ± SEM with n = 4. *****P* < 0.0001; ****P* < 0.001; **P* < 0.05. ns = not significant.

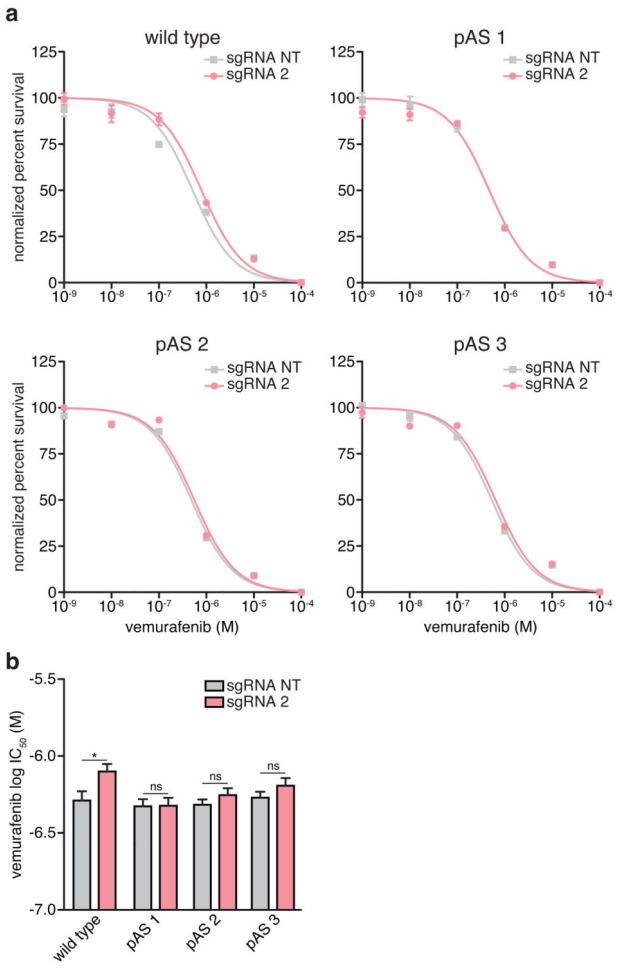

Extended Data Figure 9. Transcriptional activation of *EMICERI* confers vemurafenib resistance

a, Vemurafenib dose response curves for wild type and polyadenylation signal (pAS) clones transduced with SAM and *EMICERI*-targeting or non-targeting (NT) sgRNAs. **b,** Vemurafenib half maximal inhibitory concentration (IC50) for the same conditions as (a). All values are mean ± SEM with n = 4. **P* < 0.05. ns = not significant.

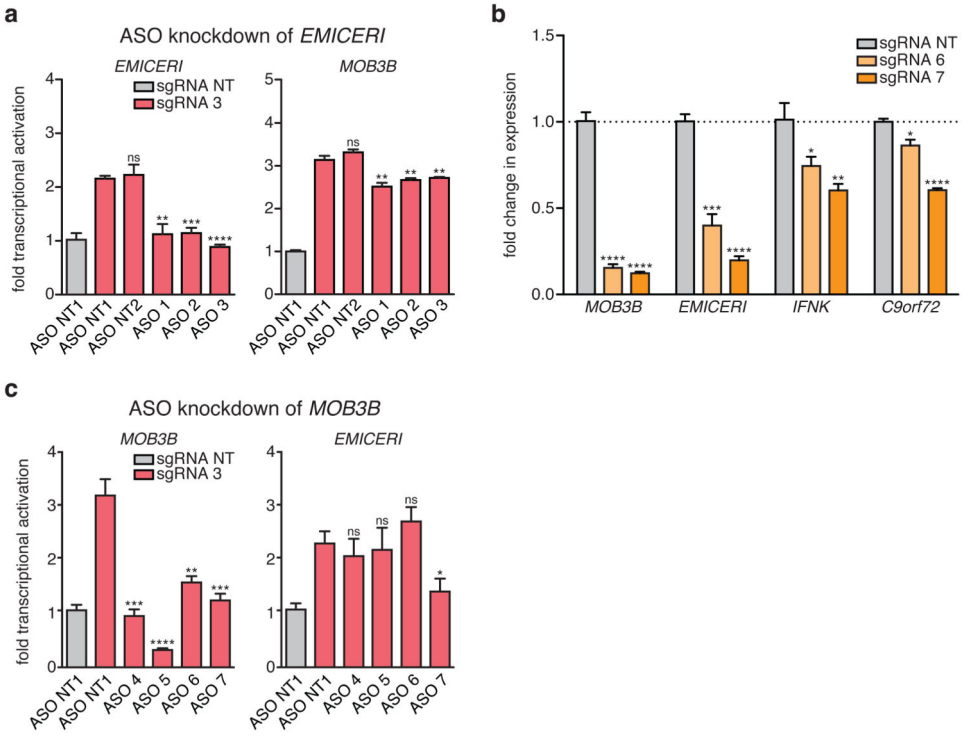

Extended Data Figure 10. *EMICERI* and *MOB3B* act reciprocally to regulate each other through the process of transcription

a, Expression of *EMICERI* and *MOB3B* after antisense oligonucleotide (ASO) knockdown of *EMICERI* in the context of SAM activation. **b,** Expression of *MOB3B* and neighboring genes in A375 cells transduced with non-targeting (NT) or *MOB3B*-targeting sgRNAs and dCas9. **c,** Expression of *MOB3B* and *EMICERI* after ASO knockdown of *MOB3B* in the context of SAM activation. **c,** All values are mean ± SEM with n = 4. ****$P < 0.0001$; ***$P < 0.001$; **$P < 0.01$; *$P < 0.05$. ns = not significant.

Supplementary Material

Refer to Web version on PubMed Central for supplementary material.

Acknowledgments

We would like to thank M. Guttman, C.M. Johannessen, and M. Ghandi for helpful discussions and insights; A. Sayeed, R. Deasy, A. Rotem, and B. Izar for generating the Cancer Cell Line Factory models; R. Belliveau for overall research support; R. Macrae for critical reading of the manuscript; and the entire Zhang laboratory for support and advice. O.O.A. is supported by a Paul and Daisy Soros Fellowship, a Friends of the McGovern Institute Fellowship, the Poitras Center for Affective Disorders, and the National Defense Science and Engineering Graduate Fellowship. J.S.G. is supported by a D.O.E. Computational Science Graduate Fellowship. N.E.S. is supported by the NIH through a Pathway to Independence Award (R00-HG008171) from the National Human Genome Research Institute and a postdoctoral fellowship from the Simons Center for the Social Brain at the Massachusetts Institute of Technology. J.B.W. is supported by the NIH through a Ruth L. Kirschstein National Research Service Award (F32-DK096822). C.P.F. is supported by the National Defense Science and Engineering Graduate Fellowship. J.M.E. is supported by the Fannie and John Hertz Foundation. F.Z. is supported by the NIH through NIMH (5DP1-MH100706 and 1R01-MH110049), the Howard Hughes Medical Institute, the New York Stem Cell, Poitras, Simons, Paul G. Allen Family, and Vallee Foundations; and David R. Cheng, Tom Harriman, and B. Metcalfe. F.Z. is a New York Stem Cell Foundation-Robertson Investigator. Reagents are available through Addgene; support forums and computational tools are available via the Zhang lab website (http://www.genome-engineering.org).

References

1. Guttman M, et al. Chromatin signature reveals over a thousand highly conserved large non-coding RNAs in mammals. Nature. 2009; 458:223–227. DOI: 10.1038/nature07672 [PubMed: 19182780]
2. Cabili MN, et al. Integrative annotation of human large intergenic noncoding RNAs reveals global properties and specific subclasses. Genes Dev. 2011; 25:1915–1927. DOI: 10.1101/gad.17446611 [PubMed: 21890647]
3. Derrien T, et al. The GENCODE v7 catalog of human long noncoding RNAs: analysis of their gene structure, evolution, and expression. Genome Res. 2012; 22:1775–1789. DOI: 10.1101/gr.132159.111 [PubMed: 22955988]
4. Brown CJ, et al. The human XIST gene: analysis of a 17 kb inactive X-specific RNA that contains conserved repeats and is highly localized within the nucleus. Cell. 1992; 71:527–542. [PubMed: 1423611]
5. Engreitz JM, et al. The Xist lncRNA exploits three-dimensional genome architecture to spread across the X chromosome. Science. 2013; 341:1237973. [PubMed: 23828888]
6. Kretz M, et al. Control of somatic tissue differentiation by the long non-coding RNA TINCR. Nature. 2013; 493:231–235. DOI: 10.1038/nature11661 [PubMed: 23201690]
7. Wang KC, et al. A long noncoding RNA maintains active chromatin to coordinate homeotic gene expression. Nature. 2011; 472:120–124. DOI: 10.1038/nature09819 [PubMed: 21423168]
8. Guttman M, Rinn JL. Modular regulatory principles of large non-coding RNAs. Nature. 2012; 482:339–346. DOI: 10.1038/nature10887 [PubMed: 22337053]
9. Anderson KM, et al. Transcription of the non-coding RNA upperhand controls Hand2 expression and heart development. Nature. 2016
10. Engreitz JM, et al. Local regulation of gene expression by lncRNA promoters, transcription and splicing. Nature. 2016
11. Paralkar VR, et al. Unlinking an lncRNA from Its Associated cis Element. Mol Cell. 2016; 62:104–110. DOI: 10.1016/j.molcel.2016.02.029 [PubMed: 27041223]
12. Konermann S, et al. Genome-scale transcriptional activation by an engineered CRISPR-Cas9 complex. Nature. 2015; 517:583–588. DOI: 10.1038/nature14136 [PubMed: 25494202]
13. O'Leary NA, et al. Reference sequence (RefSeq) database at NCBI: current status, taxonomic expansion, and functional annotation. Nucleic Acids Res. 2016; 44:D733–745. DOI: 10.1093/nar/gkv1189 [PubMed: 26553804]
14. Konig R, et al. A probability-based approach for the analysis of large-scale RNAi screens. Nat Methods. 2007; 4:847–849. DOI: 10.1038/nmeth1089 [PubMed: 17828270]
15. Johannessen CM, et al. A melanocyte lineage program confers resistance to MAP kinase pathway inhibition. Nature. 2013; 504:138–142. DOI: 10.1038/nature12688 [PubMed: 24185007]
16. Lei QY, et al. TAZ promotes cell proliferation and epithelial-mesenchymal transition and is inhibited by the hippo pathway. Mol Cell Biol. 2008; 28:2426–2436. DOI: 10.1128/MCB.01874-07 [PubMed: 18227151]
17. Lin L, et al. The Hippo effector YAP promotes resistance to RAF- and MEK-targeted cancer therapies. Nat Genet. 2015; 47:250–256. DOI: 10.1038/ng.3218 [PubMed: 25665005]
18. Praskova M, Xia F, Avruch J. MOBKL1A/MOBKL1B phosphorylation by MST1 and MST2 inhibits cell proliferation. Curr Biol. 2008; 18:311–321. DOI: 10.1016/j.cub.2008.02.006 [PubMed: 18328708]
19. West S, Proudfoot NJ, Dye MJ. Molecular dissection of mammalian RNA polymerase II transcriptional termination. Mol Cell. 2008; 29:600–610. DOI: 10.1016/j.molcel.2007.12.019 [PubMed: 18342606]
20. Skalska L, Beltran-Nebot M, Ule J, Jenner RG. Regulatory feedback from nascent RNA to chromatin and transcription. Nat Rev Mol Cell Biol. 2017
21. Fulco CP, et al. Systematic mapping of functional enhancer-promoter connections with CRISPR interference. Science. 2016; 354:769–773. DOI: 10.1126/science.aag2445 [PubMed: 27708057]
22. Liu SJ, et al. CRISPRi-based genome-scale identification of functional long noncoding RNA loci in human cells. Science. 2017; 355

23. Sanjana NE, et al. High-resolution interrogation of functional elements in the noncoding genome. Science. 2016; 353:1545–1549. DOI: 10.1126/science.aaf7613 [PubMed: 27708104]
24. Zhu S, et al. Genome-scale deletion screening of human long non-coding RNAs using a paired-guide RNA CRISPR-Cas9 library. Nat Biotechnol. 2016
25. Hsu PD, et al. DNA targeting specificity of RNA-guided Cas9 nucleases. Nat Biotechnol. 2013; 31:827–832. DOI: 10.1038/nbt.2647 [PubMed: 23873081]
26. Shalem O, et al. Genome-scale CRISPR-Cas9 knockout screening in human cells. Science. 2014; 343:84–87. DOI: 10.1126/science.1247005 [PubMed: 24336571]
27. Joung J, et al. Genome-scale CRISPR-Cas9 knockout and transcriptional activation screening. Nat Protoc. 2017; 12:828–863. DOI: 10.1038/nprot.2017.016 [PubMed: 28333914]
28. Langmead B, Trapnell C, Pop M, Salzberg SL. Ultrafast and memory-efficient alignment of short DNA sequences to the human genome. Genome Biol. 2009; 10:R25. [PubMed: 19261174]
29. Li B, Dewey CN. RSEM: accurate transcript quantification from RNA-Seq data with or without a reference genome. BMC Bioinformatics. 2011; 12:323. [PubMed: 21816040]
30. Trapnell C, Pachter L, Salzberg SL. TopHat: discovering splice junctions with RNA-Seq. Bioinformatics. 2009; 25:1105–1111. DOI: 10.1093/bioinformatics/btp120 [PubMed: 19289445]
31. Rao SS, et al. A 3D map of the human genome at kilobase resolution reveals principles of chromatin looping. Cell. 2014; 159:1665–1680. DOI: 10.1016/j.cell.2014.11.021 [PubMed: 25497547]
32. Consortium, E. P. An integrated encyclopedia of DNA elements in the human genome. Nature. 2012; 489:57–74. DOI: 10.1038/nature11247 [PubMed: 22955616]
33. Grant CE, Bailey TL, Noble WS. FIMO: scanning for occurrences of a given motif. Bioinformatics. 2011; 27:1017–1018. DOI: 10.1093/bioinformatics/btr064 [PubMed: 21330290]
34. Matys V, et al. TRANSFAC and its module TRANSCompel: transcriptional gene regulation in eukaryotes. Nucleic Acids Res. 2006; 34:D108–110. DOI: 10.1093/nar/gkj143 [PubMed: 16381825]
35. Buenrostro JD, Wu B, Chang HY, Greenleaf WJ. ATAC-seq: A Method for Assaying Chromatin Accessibility Genome-Wide. Curr Protoc Mol Biol. 2015; 109:21 29 21–29. DOI: 10.1002/0471142727.mb2129s109
36. Van der Auwera GA, et al. From FastQ data to high confidence variant calls: the Genome Analysis Toolkit best practices pipeline. Curr Protoc Bioinformatics. 2013; 43:11 10 11–33. DOI: 10.1002/0471250953.bi1110s43 [PubMed: 25431634]
37. Felsenstein J, Churchill GA. A Hidden Markov Model approach to variation among sites in rate of evolution. Mol Biol Evol. 1996; 13:93–104. [PubMed: 8583911]
38. Feng J, Liu T, Qin B, Zhang Y, Liu XS. Identifying ChIP-seq enrichment using MACS. Nat Protoc. 2012; 7:1728–1740. DOI: 10.1038/nprot.2012.101 [PubMed: 22936215]
39. Dobin A, et al. STAR: ultrafast universal RNA-seq aligner. Bioinformatics. 2013; 29:15–21. DOI: 10.1093/bioinformatics/bts635 [PubMed: 23104886]
40. DeLuca DS, et al. RNA-SeQC: RNA-seq metrics for quality control and process optimization. Bioinformatics. 2012; 28:1530–1532. DOI: 10.1093/bioinformatics/bts196 [PubMed: 22539670]
41. Liberzon A, et al. Molecular signatures database (MSigDB) 3.0. Bioinformatics. 2011; 27:1739–1740. DOI: 10.1093/bioinformatics/btr260 [PubMed: 21546393]
42. Konieczkowski DJ, et al. A melanoma cell state distinction influences sensitivity to MAPK pathway inhibitors. Cancer Discov. 2014; 4:816–827. DOI: 10.1158/2159-8290.CD-13-0424 [PubMed: 24771846]
43. Barbie DA, et al. Systematic RNA interference reveals that oncogenic KRAS-driven cancers require TBK1. Nature. 2009; 462:108–112. DOI: 10.1038/nature08460 [PubMed: 19847166]
44. Barretina J, et al. The Cancer Cell Line Encyclopedia enables predictive modelling of anticancer drug sensitivity. Nature. 2012; 483:603–607. DOI: 10.1038/nature11003 [PubMed: 22460905]

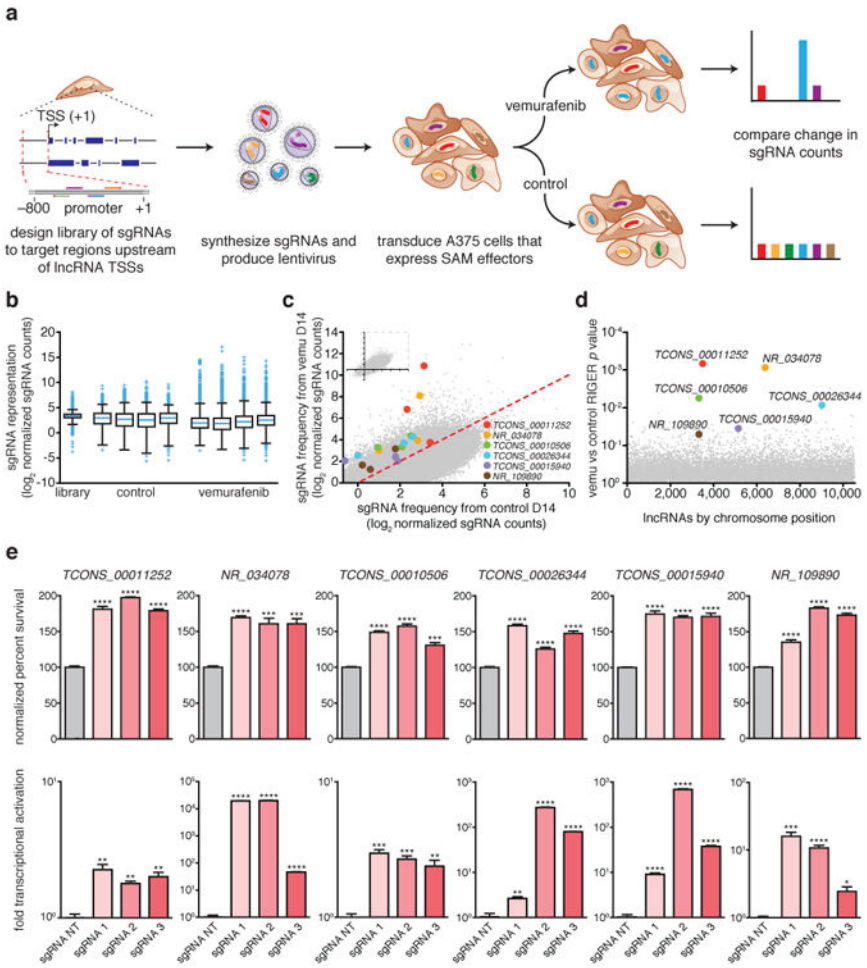

Figure 1. Genome-scale activation screen identifies lncRNA loci involved in vemurafenib resistance

a, A375 cells expressing SAM effectors are transduced with the pooled sgRNA library targeting >10,000 lncRNA TSSs and treated with BRAF inhibitor vemurafenib or DMSO (control) for 14 days. Deep sequencing identified changes in sgRNA distribution. **b,** Box plot showing the distribution of sgRNA frequencies after vemurafenib or control treatment from n = 4 infection replicates. **c,** Scatterplot showing enrichment of sgRNAs targeting 6 candidate lncRNA loci. **d,** RIGER *P* values of the candidate lncRNA loci. **e,** Validation of vemurafenib resistance and transcriptional activation in A375 cells expressing individual sgRNAs targeting 6 candidate lncRNA loci or non-targeting (NT) control sgRNA. All values are mean ± SEM with n = 4. ****$P < 0.0001$; ***$P < 0.001$; **$P < 0.01$; *$P < 0.05$.

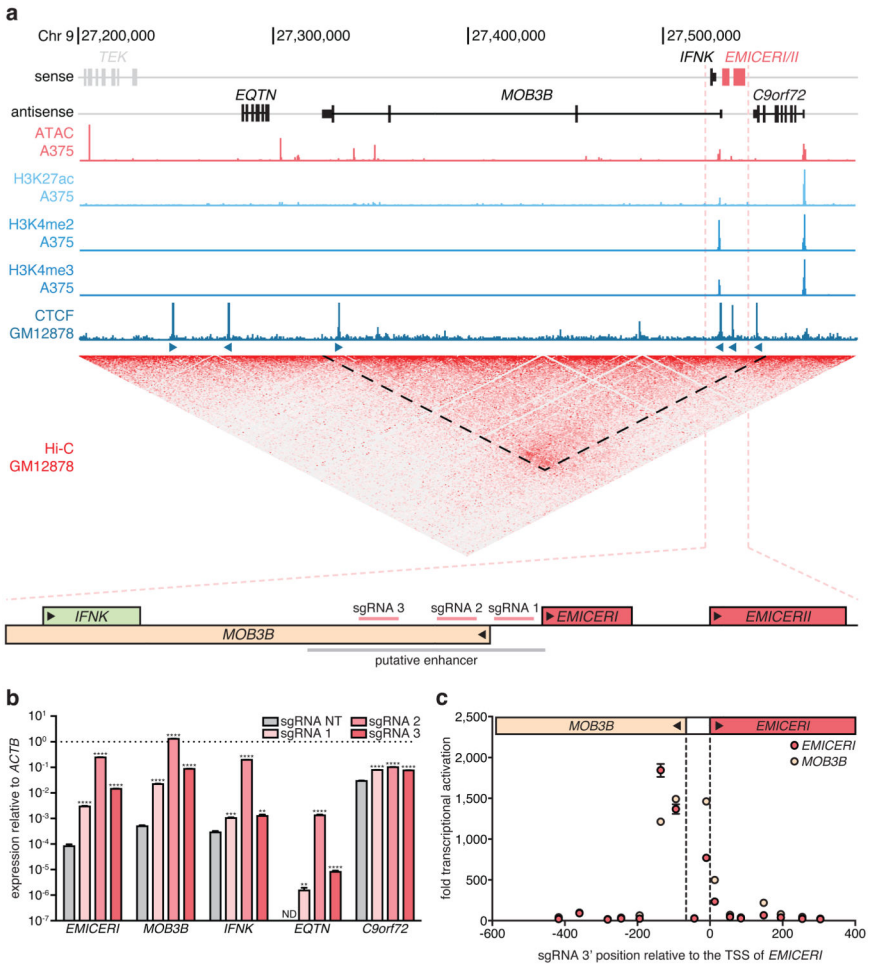

Figure 2. Activation of the *EMICERI* promoter produces dosage-dependent upregulation of neighboring genes

a, Genomic locus of *EMICERI* contains four neighboring genes (*EQTN*, *MOB3B*, *IFNK*, and *C9orf72*) and a putative enhancer. **b,** Expression of *EMICERI* and its neighboring genes after transduction with non-targeting (NT) or *EMICERI*-targeting sgRNAs and SAM. ND = not detected. **c,** Expression of *EMICERI* and *MOB3B* after transduction with sgRNAs tiling SAM across the *EMICERI* locus normalized to a NT sgRNA. All values are mean ± SEM with n = 4. ****$P < 0.0001$; ***$P < 0.001$; **$P < 0.01$.

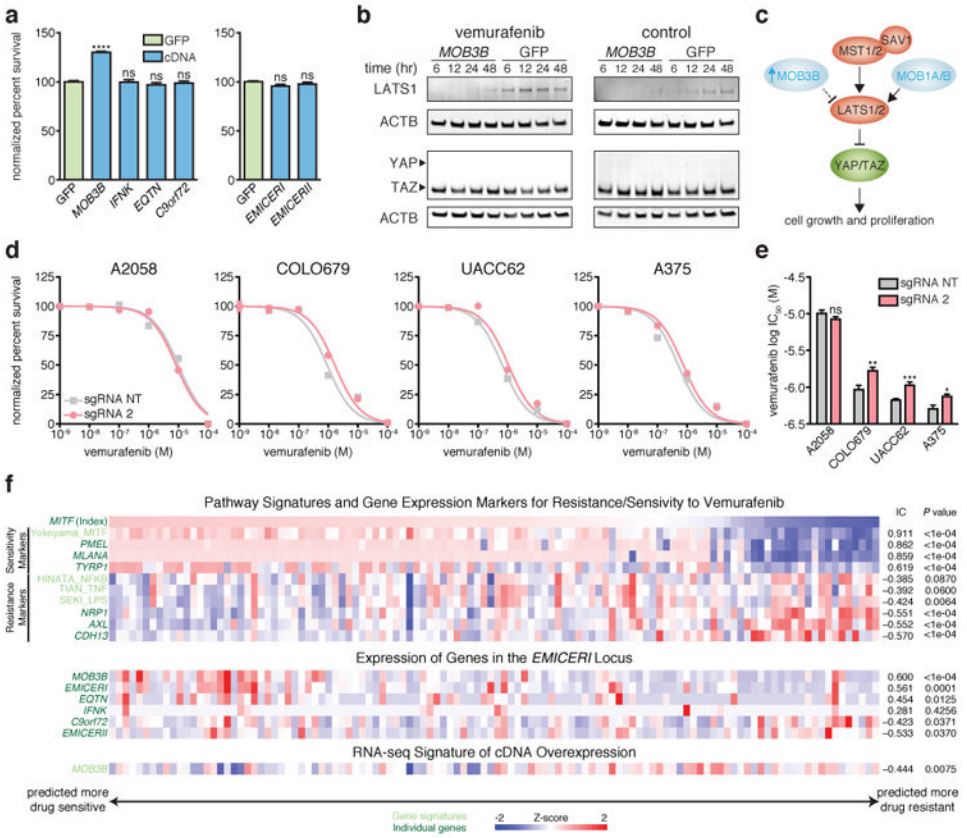

Figure 3. *MOB3B* mediates vemurafenib resistance through the Hippo signaling pathway in melanoma models

a, Vemurafenib resistance of A375 cells overexpressing each neighboring gene or lncRNA cDNA normalized to GFP. **b,** Western blots of LATS1, YAP, and TAZ in A375 stably overexpressing *MOB3B* cDNA or GFP after vemurafenib or control (DMSO) treatment. **c,** Schematic of *MOB3B* mechanism in the Hippo signaling pathway. **d,** Vemurafenib dose response curves for *EMICERI* activation in different melanoma cell lines. **e,** Vemurafenib half maximal inhibitory concentration (IC50) for the same conditions in (d). **f,** Heat map showing expression of gene/signature markers for BRAF inhibitor sensitivity (top), expression of genes in the *EMICERI* locus (middle), and *MOB3B* overexpression RNA-seq signature scores (bottom) in 113 different BRAF (V600) patient melanoma samples (primary or metastatic) from The Cancer Genome Atlas. All associations are measured using the information coefficient (IC) between the index and each of the features and *P* values are determined using a permutation test. Panels show Z scores. All values are mean ± SEM with n = 4. ****$P < 0.0001$; ***$P < 0.001$; **$P < 0.01$. *$P < 0.05$. ns = not significant.

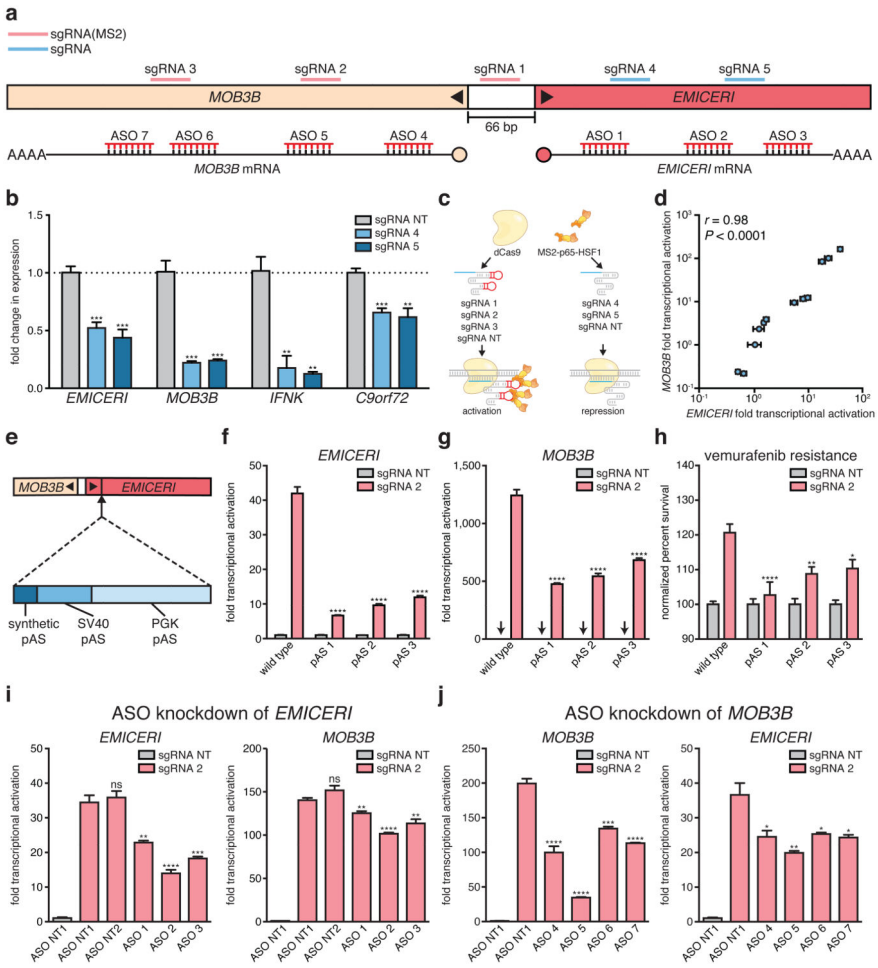

Figure 4. Transcription of *EMICERI* modulates *MOB3B* expression

a, Targeting positions of sgRNAs and antisense oligonucleotides (ASOs) in the *EMICERI* and *MOB3B* locus. **b,** Expression of *EMICERI* and its neighboring genes in A375 cells transduced with non-targeting (NT) or *EMICERI*-targeting sgRNAs and dCas9. **c,** Schematic for bimodal perturbation of *EMICERI* transcription. sgRNAs 1-3 use MS2 loops to recruit MS2-P65-HSF1 to dCas9 to activate *EMICERI*, whereas sgRNAs 4-5 recruit only dCas9 to repress *EMICERI*. **d,** Correlation between *MOB3B* and *EMICERI* expression produced by different combinations of sgRNAs with and without MS2 loops. **e,** Schematic for inserting polyadenylation signals (pAS) downstream of the *EMICERI* TSS. SV40, Simian virus 40; PGK, phosphoglycerate kinase. **f,** *EMICERI* expression after SAM activation of *EMICERI* for the wild type and pAS clones. **g,** *MOB3B* expression after the same perturbations as (f). **h,** Vemurafenib resistance after SAM activation of *EMICERI*. **i,** Expression of *EMICERI* and *MOB3B* after ASO knockdown of *EMICERI* in the context of SAM activation. **j,** Expression of *MOB3B* and *EMICERI* after ASO knockdown of *MOB3B* in the context of SAM activation. All values are mean ± SEM with n = 4. ****$P < 0.0001$; ***$P < 0.001$; **$P < 0.01$; *$P < 0.05$. ns = not significant.